Phys. Status Solidi RRL **5**, No. 3, 95–97 (2011) / **DOI** 10.1002/pssr.201004527

pss +++rapid research letters+++
www.pss-rapid.com

Direct observation of elemental segregation in InGaN nanowires by X-ray nanoprobe

J. Segura-Ruiz[*,1], G. Martinez-Criado[1], J. A. Sans[1], R. Tucoulou[1], P. Cloetens[1], I. Snigireva[1], C. Denker[2], J. Malindretos[2], A. Rizzi[2], M. Gomez-Gomez[3], N. Garro[3], and A. Cantarero[3]

[1] European Synchrotron Radiation Facility, Experiments Division, 38043 Grenoble, France
[2] Georg-August-University Göttingen, IV. Physikalisches Institut, 37077 Göttingen, Germany
[3] University of Valencia, Materials Science Institute, 46071 Valencia, Spain

Received 15 December 2010, revised 12 January 2011, accepted 13 January 2011
Published online 17 January 2011

Keywords X-ray fluorescence, X-ray nanoprobe, InGaN, nanowires

[*] Corresponding author: e-mail seguraru@esrf.fr

Using synchrotron radiation nanoprobe, this work reports on the elemental distribution in single $In_xGa_{1-x}N$ nanowires (NWs) grown by molecular beam epitaxy directly on Si(111) substrates. Single NWs dispersed on Al covered sapphire were characterized by nano-X-ray fluorescence, Raman scattering and photoluminescence spectroscopy. Both Ga and In maps reveal an inhomogeneous axial distribution inside single NWs. The analysis of NWs from the same sample but with different dimensions suggests a decrease of In segregation with the reduction of NW diameter, while Ga distribution seems to remain unaltered. Photoluminescence and Raman scattering measurements carried out on ensembles of NWs exhibit relevant signatures of the compositional disorder.

1 Introduction $In_xGa_{1-x}N$ alloy offers the possibility to tune its direct bandgap from 0.67 eV to 3.42 eV [1] providing a perfect match to the solar spectrum, which could be exploited in high-efficiency multijunction solar cells [2]. Photovoltaic efficiency could be improved further in one-dimensional core–shell NWs thanks to the orthogonalization of light absorption and radial collection of photogenerated carriers [3, 4]. The NW morphology also favors lateral elastic relaxation, allowing a larger lattice mismatch than in layers. Indeed, NWs of $In_xGa_{1-x}N$ alloys have been reported with the full compositional range [5]. However, despite the potential applications, there are only a few reports on the characterization of single $In_xGa_{1-x}N$ NWs [6] and many open questions. They refer, e.g., to the variations of indium concentration: Are such phenomena connected with phase segregation effects in the ternary alloy or compositional gradients within the nanowires? How do they affect the optical properties and vibrational order? In this work, these issues are addressed on single $In_xGa_{1-x}N$ NWs grown by molecular beam epitaxy (MBE) using hard X-ray nanoprobe, Raman scattering (RS) and photoluminescence (PL) characterization techniques.

2 Experimental details $In_xGa_{1-x}N$ NWs were grown by MBE directly on (111)Si substrates. The *ex situ* preparation of the substrate is described elsewhere [7]. The sample was grown at a substrate temperature of 480 °C under nitrogen rich condition (nitrogen flux was 1.5 sccm), with a Ga/(Ga + In) flux ratio of 0.27 and a growth time of 200 minutes. Micro-RS and PL measurements were carried out on ensembles of NWs. RS spectra were collected at room temperature with a 514.5 nm laser line and using the back-scattering configuration. PL acquisitions were performed at 7 K with a 488 nm laser line. To enable the analysis of single nanostructures, the NWs were mechanically dispersed on Al covered sapphire with a $50 \times 50\ \mu m^2$ gold grid. This grid simplifies the localization of single NWs previously observed by scanning electron microscopy (SEM). Dispersed NWs were taken from a region of about $1 \times 1\ mm^2$ in order to avoid the effects of slight dif-

ferent growth conditions. The X-ray fluorescence (XRF) measurements were collected at the nanoimaging station ID22NI of the European Synchrotron Radiation Facility. The X-ray beam was focused by a pair of KB multilayer mirrors providing a spot of 85×85 nm^2 size with a flux of 10^{12} ph/s at 17 keV ($\Delta E/E \approx 10^{-2}$) [8]. The XRF signal was detected at 15° related to the sample surface using an energy disperse silicon drift detector. The XRF spectra were analyzed using the non-linear least-squares fitting code PyMca [9].

3 Results Figure 1 shows the top and side view SEM images of the ensemble of NWs studied in the present work. The NWs are aligned along the *c*-axis of the wurtzite structure and tilted with respect to the [111] normal to the Si substrate. This tilt has been attributed to the presence of a Si_xN_y amorphous layer at the Si/$In_xGa_{1-x}N$ interface [6]. The ensemble has an average NW density of about 7×10^8 cm^{-2}, with average lengths and diameters of 700 nm and 85 nm, respectively.

Room temperature RS and 7 K PL spectra from an ensemble of NWs are shown in Fig. 2(a) and (b), respectively. The Raman spectrum displays a broad peak with its maximum around 680 cm^{-1} assigned to the A_1(LO) mode of wurtzite $In_xGa_{1-x}N$. According to the linear dependence of this vibrational mode on the Ga concentration: $A_1(LO) = x\,A_1(LO)_{InN} + (1-x)\,A_1(LO)_{GaN}$ [10], such frequency corresponds to an In content of $x = 0.35$. The other allowed mode in this configuration, E_2^h, is not observed and could be hidden by the strong peak located at 520 cm^{-1} coming from the Si substrate. The 7 K PL was acquired in an energy range from 0.56 eV to 3.44 eV. However, the emission from the NW ensemble is observed only at 735 meV within the infrared range (Fig. 2(b)). Assuming a band-to-band transition, this energy corresponds to an In content of $x = 0.95$, estimated from the bandgap variation of the ternary alloy: $E_g^{InGaN} = x\,E_g^{InN} + (1-x)\,E_g^{GaN} + x\,(1-x)\,E_b$, where $E_b = 1.43$ eV is the reported bowing parameter [11]. The resulting disagreement between RS and PL estimations is a clear signature of an extended In (Ga) inhomogeneity within the NWs. It indicates variations among different NWs in the ensemble and/or individual changes of compositional inhomogeneity inside single NWs. Such is sue can be directly addressed by hard X-ray nanoprobe,

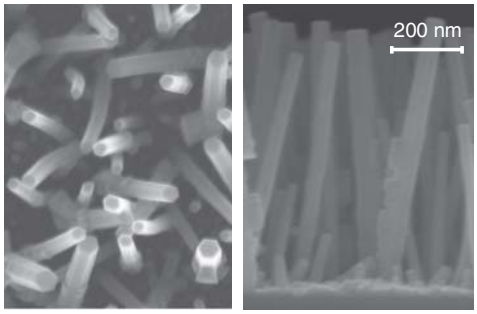

Figure 1 Top view (left) and side view (right) SEM images of the NWs ensemble.

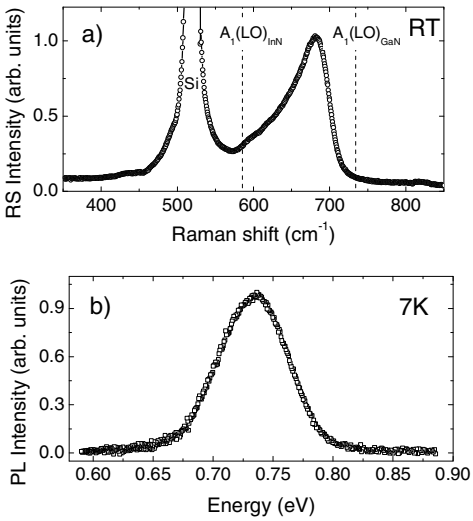

Figure 2 a) Room temperature micro-RS and b) low temperature PL spectra from the NWs ensemble.

combining high spatial resolution XRF mapping with deep escape depths and high incident photon flux.

Figure 3(a) shows the SEM micrograph of a single $In_xGa_{1-x}N$ NW. Its diameter and length are 92 nm and 585 nm, respectively. Figure 3(b) displays the XRF spectra measured on different regions (1 and 2, indicated in the SEM image) and plotted on logarithmic scale. The XRF peaks of Au, Ga and In are identified from their respective characteristic energy lines. The XRF spectra were normalized to the intensity of the Ar peaks from the air. The Au signal comes from a fraction of this element remaining on

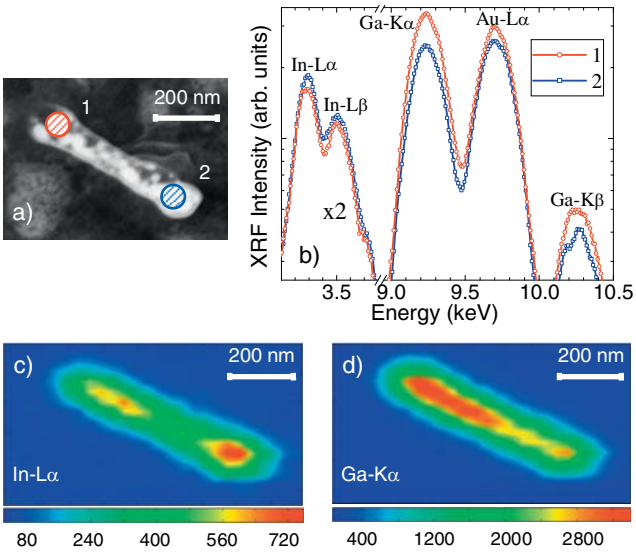

Figure 3 (online colour at: www.pss-rapid.com) (a) SEM image of a single $In_xGa_{1-x}N$ NW. (b) Normalized XRF spectra measured on regions 1 and 2 of the single NW shown in (a). The intensity has been increased by a factor 2 in the low energy side of the spectra for clarity. (c) In L_α and (d) Ga K_α fluorescence intensity maps of the same NW. The colour scale indicates the XRF intensity in photon counts.

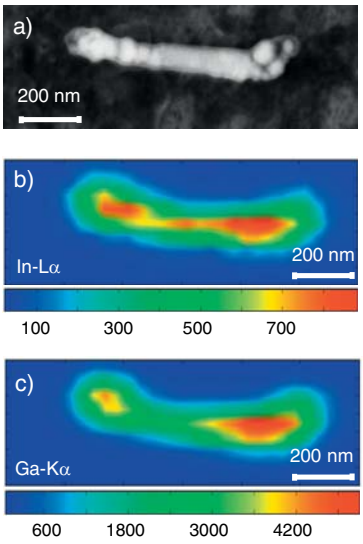

Figure 4 (online colour at: www.pss-rapid.com) (a) SEM image of a second thinner and longer NW. (b) In L_α and (c) Ga K_α fluorescence intensity maps of this second single $In_xGa_{1-x}N$ NW. The colour scale indicates the XRF intensity in photon counts.

the substrate after the photolithography process. A higher (lower) relative intensity of Ga (In) peaks in region 1 compared to region 2 is observed. This result points toward a nonuniform elemental distribution inside the single NW. Setting regions of interests around the In L_α and Ga K_α fluorescence lines, Fig. 3(c) and (d) display the respective intensity maps for the same NW taken with a 35 nm step size and an integration time of 1.5 s/point. Both spatial distributions exhibit In-rich and Ga-rich regions along the single NW, presenting flat ends without striking imperfections like nanometric steps, segment kinks or shell-like morphology. Within our experimental accuracy and length scale of the beam size, the axial change from In-rich to In-poor region is not accompanied by a significant change in diameter and/or image contrast. In the XRF map of a single NW with the characteristic baseball shape (not shown), the In accumulates at the tip of the NW, as reported for other $In_xGa_{1-x}N$ NWs [6], while Ga does at the bottom. Although the In segregation is often reported in $In_xGa_{1-x}N$ [12], our results show that this tendency is not exclusive of In atoms, but also of Ga species in these NWs grown by MBE.

Figure 4 shows the SEM image (a), and the In L_α (b) and Ga K_α (c) fluorescence intensity maps of a second longer and thinner NW belonging to the same ensemble. The diameter and the length of this NW are 76 nm and 760 nm, respectively. The XRF map was taken with a 40 nm step size and an integration time of 1.5 s/point. This NW shows Ga atoms concentrating mainly in one side of the NW. Indium concentration, on the other hand, seems to be more homogeneous along the NW than in the case of the thicker NW of Fig. 3. This behaviour suggests that a smaller diameter could reduce the In segregation in the NWs, implying a more uniform one-dimensional growth directed along the *c*-axis. From Fig. 4 is evident that In and Ga maps are not complementary as expected for a stoichiometric alloy. This behaviour suggests the existence of metallic clusters, more likely In clusters, as reported very often for InGaN layers [13]. A statistically significant number of individual NWs were characterized by X-ray nanoprobe to support the relevance of our results, showing similar findings.

In conclusion, the use of hard X-ray nanoprobe has allowed us to detect directly compositional segregations along the axial direction of single nanowires. The spatial distributions of both In and Ga elements have shown inhomogeneous incorporation preferentially at the NW ends. Our observations have indicated that smaller diameters reduce In segregation while Ga remains unaltered. All these findings explain the different Ga contents deduced from PL and RS results. In contrast to energy-dispersive X-ray studies, these results from hard X-ray nanoprobe applied to single NWs open also the possibility to study the local structure in such nanostructures.

Acknowledgements The authors thank S. Laboure for his useful help. This work was partially supported by the Grant Agreement No. 265073 – NANOWIRING of the FP7 Call of Proposals: FP7-PEOPLE-ITN-2010.

References

[1] J. Wu, W. Walukiewicz, K. M. Yu, W. Shan, J. W. Ager III, E. E. Haller, H. Lu, W. J. Schaff, W. K. Metzger, and S. Kurtz, J. Appl. Phys. **94**, 6477 (2003).
[2] X. Chen, K. D. Matthews, D. Hao, W. J. Schaff, and L. F. Eastman, Phys. Status Solidi A **205**, 1103 (2008).
[3] B. Z. Tian, X. L. Zheng, T. J. Kempa, Y. Fang, N. F. Yu, G. H. Yu, J. L. Huang, and C. M. Lieber, Nature (London) **449**, 885 (2007).
[4] K. Peng, X. Wang, and S.-T. Lee, Appl. Phys. Lett. **92**, 163103 (2008).
[5] T. Kuykendall, P. Ulrich, S. Aloni, and P. Yang, Nature Mater. **6**, 951 (2007).
[6] T. Kehagias, Physica E **42**, 2197 (2010).
[7] J. Segura-Ruiz, N. Garro, A. Cantarero, C. Denker, J. Malindretos, and A. Rizzi, Phys. Rev. B **79**, 115305 (2009).
[8] R. Tucoulou, G. Martinez-Criado, P. Bleuet, I. Kieffer, P. Cloetens, S. Labouré, T. Martin, C. Guilloud, and J. Susini, J. Synchrotron Radiat. **105**, 392 (2008).
[9] V. A. Solé, E. Papillon, M. Cotte, Ph. Walter, and J. Susini, Spectrochim. Acta B **62**, 63 (2007).
[10] H. Grille, Ch. Schnittler, and F. Bechstedt, Phys. Rev. B **61**, 6091 (2000).
[11] J. Wu, W. Walukiewicz, K. M. Yu, J. W. Ager III, E. E. Haller, H. Lu, and W. J. Schaff, Appl. Phys. Lett. **80**, 4741 (2002).
[12] A. Kar, D. Alexson, M. Dutta, and M. A. Stroscio, J. Appl. Phys. **104**, 073502 (2008).
[13] Y. L. Lai, C. P. Liu, Y. H. Lin, T. H. Hsueh, R. M. Lin, D. Y. Lyu, Z. X. Peng, and T. Y. Lin, Nanotechnology **17**, 3734 (2006).